HHS Public Access

Author manuscript

Nat Commun. Author manuscript; available in PMC 2015 May 13.

Published in final edited form as:

Nat Commun. ; 5: 5418. doi:10.1038/ncomms6418.

Inhibition of Osteoclastogenesis and Inflammatory Bone Resorption by Targeting BET Proteins and Epigenetic Regulation

Kyung-Hyun Park-Min[1,2], **Elisha Lim**[1,#], **Min Joon Lee**[1,#], **Sung Ho Park**[1], **Eugenia Giannopoulos**[1,3], **Anna Yarilina**[1], **Marjolein van der Meulen**[4,5], **Baohong Zhao**[1,2], **Nicholas Smithers**[6], **Jason Witherington**[6], **Kevin Lee**[6], **Paul P. Tak**[7], **Rab K. Prinjha**[6], and **Lionel B. Ivashkiv**[1,2,8]

[1]Arthritis and Tissue Degeneration Program and David C. Rosensweig Center for Genomics Research, Hospital for Special Surgery, New York, NY USA

[2]Department of Medicine, Weill Cornell Medical College, New York, USA

[3]Biological Sciences Department, New York City College of Technology, City University of New York, New York, USA

[4]Sibley School of Mechanical and Aerospace Engineering, Cornell University, Ithaca, USA

[5]Musculoskeletal Integrity Program, Hospital for Special Surgery, New York, NY USA

[6]Epinova DPU, GlaxoSmithKline, Medicines Research Centre, Stevenage SG1, UK

[7]Immuno-Inflammation Therapy Area, GlaxoSmithKline, Medicines Research Centre, Stevenage SG1, UK

[8]Graduate Program in Immunology and Microbial Pathogenesis, Weill Cornell Graduate School of Medical Sciences, New York, NY USA

Abstract

Emerging evidence suggests that RANKL-induced changes in chromatin state are important for osteoclastogenesis, but these epigenetic mechanisms are not well understood and have not been

Correspondence should be addressed to: Dr. Lionel B. Ivashkiv, Hospital for Special Surgery, 535 East 70th Street, New York, NY 10021; Tel. 212-606-1653; FAX 212-774-2337; IvashkivL@hss.edu; requests for I-BET151 compound should be addressed to Dr. Rab K. Prinjha at Rabinder.Prinjha@gsk.com.

[#]equal contribution

AUTHOR CONTRIBUTIONS K.-H.P.-M. conceived, designed and performed the research and wrote the manuscript. E.L. and M.J.L. performed and analyzed experiments. S.H.P., A.Y., M.M. and B.Z. contributed to the *in vivo* experiments. E.G performed bioinformatic data analysis. M.M performed and analyzed the mechanical tests. N.S. provided input into design of I-BET151 experiments and manuscript writing. K.L. initiated the collaboration. J.W. selected and provided I-BET151, advice on its use and data interpretation, and input into manuscript finalization. P.P.T. provided input into clinical significance and manuscript finalization. R.K.P. initiated the collaboration, and provided input into design and interpretation of experimental work and finalization of the manuscript. L.B.I. conceived and oversaw the project and wrote the manuscript.

COMPETING FINANCIAL INTERESTS K.-H.P.-M., E.L., M.J.L., S.H.P., E.G., A.Y., B.Z. and L.B.I. declare no competing financial interests. N.S., K.L., J.W., P.P.T and R.K.P. are current or former employees of Glaxo Smith Kline and hence hold shares. GSK is testing BET Bromodomain inhibitors in clinical trials.

therapeutically targeted. In this study we find that the small molecule I-BET151 that targets bromo and extra-terminal (BET) proteins that “read” chromatin states by binding to acetylated histones strongly suppresses osteoclastogenesis. I-BET151 suppresses pathologic bone loss in TNF-induced inflammatory osteolysis, inflammatory arthritis, and post-ovariectomy models. Transcriptome analysis identifies a MYC-NFAT axis important for osteoclastogenesis. Mechanistically, I-BET151 inhibits expression of the master osteoclast regulator NFATC1 by suppressing expression and recruitment of its newly identified upstream regulator MYC. MYC is elevated in rheumatoid arthritis and its induction by RANKL is important for osteoclastogenesis and TNF-induced bone resorption. These findings highlight the importance of an I-BET151-inhibited MYC-NFAT axis in osteoclastogenesis, and suggest targeting epigenetic chromatin regulators holds promise for treatment of inflammatory and estrogen deficiency-mediated pathologic bone resorption.

Introduction

Osteoclasts are bone-resorbing cells important for bone homeostasis and pathological bone resorption [1–5]. M-CSF and RANKL are key factors required for differentiation of myeloid lineage cells into osteoclasts. M-CSF promotes proliferation and survival of myeloid cells and induces expression of RANK, the receptor for the key inducer of osteoclastogenesis RANK ligand (RANKL). RANKL drives osteoclast differentiation by activating NF-κB, MAPK and calcium signaling pathways to induce and activate transcription factor NFATc1, a master regulator of osteoclastogenesis. RANKL-mediated signaling pathways are well characterized [1] and RANKL-RANK interactions and downstream signaling pathways have been targeted to treat osteoporosis and other bone diseases. Recently, it has become apparent that RANKL-induced changes in chromatin state of osteoclast precursors are important for osteoclastogenesis [6,7]. However, epigenetic mechanisms that regulate osteoclast differentiation have not been well clarified or therapeutically targeted.

Epigenetic regulation, which includes modifications of DNA and chromatin, and expression of noncoding RNA, plays an important role in physiological responses and pathological conditions [8–10]. Recent development of drugs that target epigenetic mechanisms, including chromatin states, holds great promise in treating diseases such as cancers [11,12]. Bromodomain and extra-terminal (BET) proteins “read” chromatin states by binding to acetylated histones (H-Ac) via bromodomains, and recruit additional chromatin regulators to control gene transcription [13]. Small molecule inhibitors which target the BET family have been generated and inhibition of interaction of BET proteins with H-Ac using small molecule inhibitors effectively suppresses tumor growth and inflammatory responses in mouse models [13–19]. These inhibitors show high specificity for their targets, specifically binding the BET family proteins, and minimal systemic toxicity, suggesting a high potential as effective and safe therapeutics [11,14,15,20]. Here, we report that the small molecule inhibitor I-BET151 that targets BET proteins effectively suppresses RANKL-induced osteoclastogenesis. I-BET151 treatment suppressed *in vivo* bone loss in post ovariectomy osteoporosis, inflammatory arthritis, and TNF-induced osteolysis mouse models. Transcriptome analysis revealed that I-BET 151 inhibits NFATc1 expression by suppressing MYC, and we identified a MYC-NFAT axis important for osteoclastogenesis that is targeted

by I-BET151. These findings implicate MYC and BET proteins in osteoclastogenesis, and suggest targeting epigenetic chromatin regulators as a new therapeutic approach for controlling inflammatory bone resorption.

Results

I-BET151 suppresses osteoclastogenesis in vitro and in vivo

We tested the effects of BET bromodomain protein inhibition on osteoclast differentiation. I-BET151 suppressed the differentiation of human and mouse osteoclast precursors (OCPs) into multinucleated tartrate-resistant acid phosphatase (TRAP)-positive cells in a dose-dependent manner (Fig. 1a and Supplementary Fig. 1a). Accordingly, I-BET151 strongly suppressed RANKL-induced expression of osteoclast-related genes such as *CTSK* (encodes cathepsin K) and *ITGB3* (encodes β3 integrin) in human and mouse OCPs (Fig. 1b and Supplementary Fig. 1b). Reduced osteoclast formation did not result from changes in cell viability or number, as assessed by MTT assays (Supplementary Fig. 2a, b). We next tested whether I-BET151 could inhibit osteoclastogenesis *in vivo*. I-BET151 strongly inhibited osteoclastogenesis and associated bone erosion *in vivo* in the TNF-induced supracalvarial osteolysis model (Fig. 1c). Consistently, serum TRAP levels were lower in the I-BET151 treated group compared to the vehicle-treated control group (Fig. 1d). The reduction in *in vivo* osteoclastogenesis was further confirmed using histomorphometric analysis to quantify osteoclast numbers and surface area; both osteoclast surface area per bone surface (OcS/BS) and osteoclast numbers per bone surface (NOc/BS) were significantly lower in the I-BET151-treated group (Fig. 1e). Collectively, our results show that I-BET151 suppressed osteoclastogenesis *in vitro* and *in vivo*.

I-BET151 protects mice from bone loss in OVX and arthritis

To further test the efficacy of inhibiting BET proteins in the treatment of pathological bone loss, we examined the effect of I-BET151 on bone loss in post-ovariectomy (OVX) osteoporosis using a therapeutic experimental design. I-BET151 treatment was started four weeks after OVX and continued for five weeks (Fig. 2a). Microcomputed tomography (μCT) analysis revealed that I-BET151 treatment resulted in significantly increased bone mass relative to vehicle-treated mice (Fig. 2b, c). Biomechanical properties of the femurs were assessed by three-point bending and I-BET151 resulted in significantly increased bone strength compared to vehicle treated ovariectomized mice (Fig. 2d). Histomorphometry showed that I-BET151 decreased osteoclast numbers and surface area, supporting a suppressive effect of I-BET151 on osteoclastogenesis (Fig. 2e). Consistent with previous observations [21], the effects of I-BET in the OVX model with a therapeutic design were similar to those of alendronate (Supplementary Fig. 3), a well-known anti-resorptive reagent that targets osteoclasts with minimal direct effects on osteoblasts[22]. However, we tested the effects of I-BET151 on osteoblast function. At the doses used to suppress osteoclastogenesis *in vivo*, I-BET151 treatment did not significantly affect mineral apposition rate (MAR) and bone formation rate (BFR) in ovariectomized mice (Supplementary Fig. 4). However, I-BET151 suppressed *in vitro* osteoblast differentiation at concentrations 5-10-fold higher than those required to suppress osteoclastogenesis (Supplementary Fig. 5). Thus, our results suggest that I-BET151 therapeutically increases bone mass in the OVX model by

suppressing osteoclastogenesis, but that supra-therapeutic doses have the potential to suppress osteoblast-mediated bone formation.

We next tested the effects of I-BET151 in K/BXN serum-induced arthritis, which models the inflammatory effector phase of arthritis and is characterized by joint inflammation and associated bone resorption [23]. I-BET151-treated mice showed decreased joint swelling and inflammation compared to vehicle-treated control mice (Fig. 3a, b and Supplementary Fig. 6). I-BET151-treated mice also showed decreased serum TRAP and decreased osteoclast numbers in periarticular bone (Fig. 3c–e). K/BXN serum-induced arthritis is induced by articular immune complexes and is highly dependent on interleukin-1 (IL-1)[24] and chemokine-mediated recruitment of neutrophils [25]. To gain insights into how I-BET151 inhibits arthritic inflammation, we found that I-BET151 suppresses the induction of IL-1 by immune complexes and various inflammatory stimuli, and also attenuates induction of neutrophil chemokines by immune complexes or IL-1 (Supplementary Fig. 7). These results suggest that in the K/BXN arthritis model, I-BET151 potently suppresses bone resorption by a dual action of suppressing inflammation and directly targeting osteoclast differentiation. Taken together, our results establish *in vivo* efficacy of I-BET151 and suggest that inhibition of BET proteins may represent an effective therapeutic approach for suppressing bone loss.

I-BET151 suppresses RANKL-induced NFATc1 expression

To test in an unbiased manner for potential targets of I-BET151 that could yield insight into its mechanisms of action, we performed a transcriptomic analysis using high throughput RNA sequencing (Supplementary Fig. 8). I-BET151 suppressed expression of 465 RANKL-induced genes by >50% in two independent donors. These genes are depicted in the heat map in Fig. 4a and listed in Supplementary Table 1; Supplementary Figs. 9–11 and legends describe our analysis of transcriptomic data. Strikingly, of the 465 I-BET151 targets, 120 genes (26%) are target genes of the master regulator of osteoclastogenesis *NFATC1*[26] (Supplementary Table 2), and expression of *NFATC1* itself was suppressed (Fig. 4a). NFATc1 drives the early stages of osteoclast differentiation [27–29], NFATc1-deficient mice develop severe osteopetrosis *in vivo* [30], and NFATc1-deficient cells are incapable of differentiating into osteoclasts *in vitro* [28,29,31]. Thus, we focused on understanding how I-BET151 suppresses *NFATC1* to downregulate osteoclastogenesis. In both human and mouse OCPs, RANKL-induced NFATc1 mRNA and protein expression were inhibited by I-BET151 in a dose-dependent manner (Fig. 4b, c and Supplementary Fig. 12a, b). I-BET151 also suppressed RANKL-induced expression of Blimp1, another key regulator of osteoclastogenesis that is induced in part by NFATc1[32,33] (Fig. 4c and Supplementary Fig. 12a). Downregulation of *NFATC1* expression by I-BET151 was not secondary to inhibition of upstream RANK signaling (Supplementary Fig. 13a) or induction of known transcriptional repressors of *NFATC1* and osteoclast differentiation (Supplementary Fig. 13b), suggesting that I-BET151 either directly targets the *NFATC1* locus or suppresses an as yet unknown activator of *NFATC1*.

We next investigated mechanisms by which I-BET151 inhibits *NFATC1* expression. I-BET151 directly inhibits gene expression by disrupting binding of BET proteins to gene loci[14]. However, using chromatin immunoprecipitation (ChIP) assays, we found that

RANKL stimulation resulted in only a modest and not statistically significant recruitment of BET proteins such as Brd4 to the *NFATC1* locus (Fig. 4d). Although suppression of Brd4 recruitment (Fig. 4d) could contribute to suppression of NFATC1 expression, the weak recruitment of Brd4 suggested that I-BET151 could also regulate *NFATC1* expression indirectly, potentially by suppressing the expression of a transcriptional activator required for *NFATC1* transcription. Such an indirect mechanism of action was supported by the finding that I-BET suppressed RANKL-induced increases in the positive histone mark H4-Ac at the *NFATC1* locus (Fig. 4e), and, concomitantly, RANKL-induced recruitment to *NFATC1* of CBP, a key histone acetyltransferase (HAT) that mediates histone acetylation (Fig. 4f). Decreased recruitment of CBP to the *NFATC1* promoter suggests that I-BET151 may suppress a RANKL-induced transcription factor that is required to recruit HATs to acetylate histones at *NFATC1*.

MYC-NFATc1 axis is important for osteoclast differentiation

Although the currently appreciated important transcriptional regulators of osteoclastogenesis[34] are not known BET targets (Fig. 4a and Supplementary Fig. 13), the transcription factor MYC is dependent on BET proteins [18,35] and was suggested to play a role in osteoclastogenesis in RAW267.4 cells and mouse osteoclasts [36,37]; however, mechanisms by which MYC regulates osteoclastogenesis remain to be elucidated. Strikingly, analysis of our transcriptomic data showed that 73 out of 465 (16%) of I-BET targets correspond to MYC target genes (Supplementary Fig. 10), that MYC-dependent cellular processes were suppressed by I-BET (Supplementary Figs. 9 and 11) and that MYC- and NFAT-target genes overlap (Supplementary Fig. 10). These results support the idea that a MYC-NFATC1 axis is important for osteoclastogenesis and thus we addressed the role of MYC in our system. RANKL induced MYC (Fig. 5a) with similar kinetics as induction of NFATc1 (Supplementary Fig. 14). I-BET151 abrogated RANKL-induced MYC expression in human and mouse OCPs (Fig. 4a, 5a and Supplementary Fig. 15). To examine the role of MYC in human OCPs, we treated cells with MYC inhibitor 10058-F4 [38] or knocked down MYC expression using siRNAs. Inhibition of MYC suppressed osteoclast differentiation (Fig. 5b). We then tested whether MYC regulates the expression of *NFATC1*. MYC inhibitor 10058-F4 inhibited RANKL-induced NFATC1 mRNA and protein expression in dose-dependent manner in human and mouse OCPs (Fig. 5c, d and Supplementary Fig. 16). Consistently, siRNA-mediated knockdown of MYC inhibited osteoclastogenesis and RANKL-induced NFATc1 expression (Supplementary Fig. 17). Furthermore, ChIP assays showed that RANKL stimulation induced recruitment of MYC to the *NFATC1* promoter, supporting direct regulation of *NFATC1* by MYC (Fig. 5e). This RANKL-induced occupancy of MYC at the *NFATC1* promoter was effectively suppressed by I-BET151 (Fig. 5e). Inhibition of MYC decreased RANKL-induced H4-Ac at the *NFATC1* promoter (Fig. 5f) in a manner parallel to decreased H4-Ac after I-BET151 treatment (Fig. 4e). These results indicate that MYC is required for the induction of H4-Ac at the *NFATC1* promoter. Accordingly, MYC inhibition resulted in similar decreases in RANKL-induced recruitment of CBP to *NFATC1* (Fig. 5g). These results establish inhibition of MYC as a mechanism by which I-BET151 regulates *NFATC1*, and support a role for MYC in osteoclastogenesis. We previously reported that the expression of NFATC1 protein is increased in synovial OCPs of rheumatoid arthritis (RA) patients [39], which have a higher potential for differentiating into

osteoclasts [40]. To investigate a potential role for MYC *in vivo*, we first examined MYC expression in RA synovial OCPs. Quantitative RT-PCR analysis showed significantly increased MYC expression in RA synovial $CD14^+$ OCPs relative to disease controls, and a parallel increase in NFATC1 mRNA (Fig. 5h). These results suggested a role for MYC in osteoclastogenesis in inflammatory settings, which we further investigated using the TNF-induced supracalvarial osteolysis model. Similar to I-BET151 treatment, the MYC inhibitor 10058-F4 suppressed TNF-induced serum TRAP (Fig. 5i) and significantly reduced both osteoclast surface area per bone surface (OcS/BS) and osteoclast numbers per bone surface (NOc/BS) (Fig. 5j). Taken together, these results reveal MYC as an important factor in osteoclastogenesis and suggest targeting MYC as a new therapeutic strategy to control bone resorption.

Discussion

Cytokines, receptors, signaling pathways and transcription factors that regulate osteoclastogenesis have been extensively characterized [1,41], resulting in the identification of therapeutic targets, such as RANKL and NFATC1, for the treatment of pathological bone resorption [2–4]. Emerging evidence suggests that chromatin states and related epigenetic mechanisms that control how information encoded in DNA is expressed play an important role in osteoclastogenesis [6,7,31]. As many chromatin regulators are enzymes or ‘readers’ that can be targeted by conventional small molecule approaches [11], this opens up new therapeutic opportunities for suppression of osteoclastogenesis and pathologic bone resorption. In this study, we show that I-BET151 inhibits osteoclast differentiation and suppresses *in vivo* osteoclastogenesis and pathologic bone resorption in three distinct disease models: TNF-induced inflammatory osteolysis, inflammatory arthritis, and post ovariectomy low estrogen-mediated osteoporosis. Mechanistically, I-BET151 inhibited expression of the master osteoclast regulator *NFATC1* by suppressing expression and recruitment of its upstream regulator MYC. MYC was elevated in rheumatoid arthritis synovial macrophages and its induction by RANKL was important for osteoclastogenesis and TNF-induced bone resorption. These results highlight the importance of an I-BET151-inhibited MYC-NFATC1 axis in osteoclastogenesis and pathologic bone resorption.

Epigenetic mechanisms contribute to regulation of the expression of genes, and therapies targeting epigenetic marks including DNA methylation and histone modifications such as acetylation and methylation show therapeutic efficacy in several diseases and various disease models[11,12]. In preclinical studies the related compounds I-BET151 and I-BET762, and JQ1, appear safe and highly efficacious in treatment of NUT midline carcinoma, acute myeloid leukemia, and multiple myeloma [15,18,42] and I-BET762[14] is currently in clinical trials (clinicaltrials.gov reference NCT01587703). We have demonstrated therapeutic efficacy of I-BET151, a compound that targets an epigenetic mechanism important for osteoclastogenesis, in increasing bone mass and strength in the standard post OVX model of osteoporosis. While our manuscript was under revision, the related BET inhibitor JQ1 was reported to suppress osteosarcoma-mediated bone remodeling by suppressing the function of both osteoclasts and osteoblasts [43]. As we have found that 5-10-fold higher concentrations of I-BET151 are required to suppress osteoblast differentiation than osteoclastogenesis (Supplementary Figs. 1 and 5), the differences in results, namely the lack of suppression of

osteoblast function in vivo in our study, may be explained by differences in dosing or pharmacokinetics of these two BET inhibitors. Alternatively, it is possible that distinct pathogenic mechanisms in inflammatory or low estrogen-mediated bone loss versus tumor-mediated bone remodeling[5] result in differential responses to BET inhibitors. Overall our results in the post-ovariectomy model that I-BET151 suppressed osteoclastogenesis and bone resorption but minimally affected bone formation suggest a therapeutic window in which I-BET151 can exert beneficial effects on bone mass.

I-BET151 effectively suppressed osteoclastogenesis and pathologic bone resorption in inflammatory disease models. Inflammatory bone resorption can be refractory to established antiresorptive therapies [3,44], such as bisphosphonates, that target osteoclasts. In the K/BxN arthritis model, I-BET151 suppressed inflammation as well as bone resorption. Thus, I-BET151 offers the advantage of both suppressing inflammation, thus indirectly dampening osteoclastogenesis, and directly suppressing osteoclast differentiation. BET inhibitors have been shown to suppress induction of inflammatory secondary response genes by bacterial lipopolysaccharide (LPS)[14] and we have extended this work to show that I-BET151 suppresses immune complex- and IL-1-induced expression of cytokines and neutrophil chemoattractants that are important for inflammatory arthritis. The combined effect of suppressing inflammation and osteoclastogenesis suggests targeting BET proteins may be effective in suppressing pathological bone resorption that occurs in inflammatory settings.

BET inhibitors may have different therapeutic targets in various diseases[11]. One such target is MYC and BET inhibitors have therapeutic applications in MYC-driven disorders, which have otherwise been refractory to various therapeutic strategies to target MYC. Our results suggest that in osteoclasts I-BET151 works at least in part by suppressing MYC and targeting a newly described MYC-NFAT axis important for osteoclastogenesis. MYC has been previously implicated in osteoclastogenesis but the mechanism by which MYC regulates osteoclastogenesis was not clear[36,37]. Our investigation of mechanisms of I-BET151 action revealed a role for MYC in osteoclast differentiation and inflammatory bone resorption. One mechanism of MYC action was direct binding to and activation of *NFATC1* expression, although it is possible that MYC also promotes osteoclastogenesis by additional mechanisms that remain to be investigated. In summary, our results on the importance of BET proteins and MYC in osteoclastogenesis open new lines of investigation in the understanding and therapeutic targeting of pathological bone resorption.

Methods

Mice and analysis of bone phenotype

Six week-old female C57BL/6 were purchased from The Jackson Laboratory (Bar Harbor, ME). All animal experiments were approved by the Hospital for Special Surgery Institutional Animal Care and Use Committee (IACUC). All animals were randomly assigned into experimental groups. For ovariectomy (OVX) -induced bone loss model, sixteen week-old sham-operated or ovariectomized CD-1 mice were purchased from Charles River Laboratory (Wilmington, MA). I-BET151 was prepared in 10% KLEPTOSE® (Roquette Pharma) following the manufacturer's instructions. Ovariectomized mice were randomly divided into two groups (vehicle vs. I-BET; n=12 per group). To analyze the

therapeutic effect of I-BET151, either vehicle or I-BET151 (30mg kg^{-1}) was administrated intraperitoneally (i.p.) once per day beginning 4 weeks after surgery. I-BET151 or vehicle injection was continued for five weeks. After five-week treatment, femurs were isolated and micro–computed tomography (μ-CT) analysis[45] was performed at the Musculoskeletal Repair and Regeneration Core Center in Hospital for Special Surgery as described previously [46], and all samples were included in the analysis conducted in a blinded manner. For arthritis experiments, K/BxN serum pools were prepared as described previously[47]. Arthritis was induced by intraperitoneal injection of 100 μl of K/BxN serum on days 0 and 2. Arthritic mice were divided into 2 groups (vehicle vs. I-BET151; n=9 mice per group) and were administered vehicle or I-BET151 (40 mg kg^{-1}) once on days 0 and 2 and twice per day from day 3 to day 6. Control group (n=9) only received vehicle but not arthritic serum. The severity of arthritis was monitored by measuring the thickness of both the wrist and ankle joints using dial-type calipers (Bel-Art Products). For each animal, joint thickness was calculated as the sum of the measurements of both wrists and both ankles. Joint thickness was represented as the average for every treatment group. For inflammatory osteolysis experiments, we used an established mouse model, the TNF-induced supracalvarial osteolysis model [48] with minor modifications. In brief, TNF was administrated daily at the doses indicated in the figure legends to the calvarial periosteum of mice for four to five consecutive days. The mice were then sacrificed for the collection of serum and calvarial bones for sectioning. For histopathologic assessment, mice were euthanized, and the hind paws and calvarial bones were harvested and fixed in 4% paraformaldehyde for 2 days. These samples were decalcified with 10% neutral buffered EDTA (Sigma-Aldrich) and embedded in paraffin. To assess osteoclastogenesis and bone resorption, sections were stained with TRAP (tartrate-resistant acid phosphatase) and hematoxylin for osteoclast visualization, and histomorphometric analysis was performed with the BioQuant image analysis system (Nashville, TN, USA) using standard procedures [49]. Osteoclasts were identified as $TRAP^+$ cells that were multinucleated and adjacent to bone. As markers for osteoclast formation and bone resorption, serum TRAP5b was measured with the RatLaps enzyme immunoassay (EIA) kit (Immunodiagnostic Systems) following the manufacturer's instructions.

Three-point bending test

The whole bone strength of the femur was measured in bending. Femurs were loaded in three-point bending to failure[50]. The bones were positioned with the posterior aspect resting on the supports (6 mm span) and the load was applied to the anterior mid-diaphysis at a rate of 0.1 mm/s (Bose Enduratec). The bending strength (maximum moment) and stiffness were determined from the applied load and displacement data. All samples were included in the analysis conducted in a blinded manner.

Reagents

Human and murine M-CSF, sRANKL and TNF were purchased from Peprotech (Rocky Hill, NJ). I-BET was synthesized by GlaxoSmithKline (UK) as previously described[15,51,52]. MYC inhibitor 10058-F4 was purchased from Sigma-Aldrich. The MTT assay kit was purchased from Roche, and cell viability was measured following the manufacturer's instructions. The antibodies (1:1000) used for immunoblotting are as follows: NFATc1(BD

Pharmagen; 556602); c-myc and p38 (Santa Cruz Biotechnology; sc-764 and sc535); Lamin B (Abcam; ab16048); phospho-ERK, IκBα, phospho-p38 and Blimp1 (Cell Signaling; 9101, 9242, 9215, 9115).

Cell culture

Peripheral blood mononuclear cells were obtained from blood leukocyte preparations purchased from the New York Blood Center by density gradient centrifugation with Ficoll (Invitrogen, Carlsbad, CA) using a protocol approved by the Hospital for Special Surgery Institutional Review Board. Monocytes were obtained from peripheral blood using anti-CD14 magnetic beads, as recommended by the manufacturer (Miltenyi Biotec Auburn, CA). Monocyte-derived osteoclast precursors (OCPs) that express RANK were obtained by culturing for one day with 20 ng ml^{-1} of M-CSF (Peprotech) in α-MEM medium (Invitrogen) supplemented with 10 % fetal bovine serum (FBS, Hyclone), and the purity of monocytes was >97%, as verified by flow cytometric analysis.

Osteoclast differentiation

Human $CD14^+$ cells were incubated with 20 ng ml^{-1} of M-CSF for one day to generate OCPs. For human osteoclastogenesis assays, cells were added to 96 well plates in triplicate at a seeding density of 5×10^4 cells per well. Osteoclast precursors were incubated with 20 ng $ml^{-1}$of M-CSF and 40 ng $ml^{-1}$of human soluble RANKL for five additional days in α-MEM supplemented with 10 % FBS. Cytokines were replenished every 3 days. On day 6, cells were fixed and stained for TRAP using the Acid Phosphatase Leukocyte diagnostic kit (Sigma) as recommended by the manufacturer. Multinucleated (greater than 3 nuclei), TRAP-positive osteoclasts were counted in triplicate wells. For mouse osteoclastogenesis, bone marrow (BM) cells were flushed from femurs of mice and cultured with murine M-CSF (20 ng ml^{-1}, Peprotech) on petri dishes in α-MEM supplemented with 10% FBS after lysis of RBCs using ACK lysis buffer (Cambrex, Walkersville, MD). Then, the non-adherent cell population was recovered the next day and cultured with murine M-CSF (20 ng ml^{-1}) for three additional days. We defined this cell population as mouse OCPs. For murine osteoclastogenesis assays, we plated 2×10^4 OCPs per well in triplicate wells on a 96 well plate and added M-CSF and RANKL (100 ng ml^{-1}) for an additional 6 days, with exchange of fresh media every 3 days. Imaging was performed with a 10X objective.

Gene expression analysis

For real time PCR, DNA-free RNA was obtained using the RNeasy Mini Kit from QIAGEN with DNase treatment, and 0.5 μg of total RNA was reverse transcribed using a First Strand cDNA Synthesis kit (Fermentas, Hanover, MD). Real time PCR was performed in triplicate using the iCycler iQ thermal cycler and detection system (Applied Biosystems, Carlsbad, CA) following the manufacturer's protocols. Expression of the tested gene was normalized relative to levels of GAPDH.

RNA-sequencing

Total RNA was first extracted using RNeasy mini kit (Qiagen). True-seq sample preparation kits (Illumina) were then used to purify poly-A transcripts and generate libraries with

multiplexed barcode adaptors. All samples passed quality control analysis on a Bioanalyzer 2100 (Agilent). Paired-end reads (50 × 2 cycles, ~75×10^6 reads per sample) were obtained on an Illumina HiSeq 2500/1500 in the Weill Cornell Medical College Genomics Resources Core Facility. The TopHat program (v 1.2.0) was used to align the reads to the UCSC Hg19 human reference genome, while the Cufflinks program (v. 0. 93) allowed for measurements of transcript abundance (represented by Fragments Per Kilobase of exon model per Million mapped reads (FPKM)). Genes and transcripts with FPKM values lower than five were not included in the analysis. Pearson correlation analysis and heatmaps was generated using R (3.0.2). The RNA sequencing data have been deposited to the Sequence Read Archive (http://www.ncbi.nlm.nih.gov/sra/) and assigned study number SRP047069.

Chromatin Immunoprecipitation (ChIP)

ChIP was performed as previously described [14]. Briefly, 2×10^7 human primary OCPs were fixed by adding formaldehyde directly to the medium to a final concentration of 1 % for 5 min. Cells were harvested, washed, and lysed. Chromatin was sheared by sonication to a length of approximately 500 base pairs using a Bioruptor sonicator (Diagenode). Sheared chromatin was precleared and then immunoprecipitated with antibodies; c-myc (Abcam; ab56), Brd4 (Bethyl Lab; A301-985A), pan acetyl-H4 (Millipore; 06-866), and CBP (Abcam; ab2832). Immune complexes were subsequently collected and washed, and DNA crosslinking was reversed by heating at 65°C overnight. Following proteinase K digestion, DNA was recovered using the PCR purification kit (Qiagen) and real time PCR was performed to detect the occupancy of target proteins. Signals obtained from the ChIP are divided by signals obtained from an input sample. This input sample represents the amount of chromatin used in the ChIP. The primer sequences are listed in Supplementary Table 3.

Statistical analysis

All statistical analyses were performed with Graphpad Prism 5.0 software using the 2-tailed, unpaired *t*-test (two conditions), one-way or two-way ANOVA for multiple comparisons (more than two conditions) with posthoc Tukey test. $p<0.05$ was taken as statistically significant.

Supplementary Material

Refer to Web version on PubMed Central for supplementary material.

Acknowledgments

We thank Hospital for Special Surgery rheumatologists for providing synovial specimens, Angela Lee for processing samples, Lyudmila Lukashova in the Musculoskeletal Repair and Regeneration Core Center for micro-CT analysis, Dr. Steven Doty in the Analytical Microscopy Core, Drs. Steve Goldring, Adele Bosky, and George Kalliolias for helpful discussions, and Dr. Laura Donlin for critical review of the manuscript. This study was supported by the National Institute of Arthritis and Musculoskeletal and Skin Diseases (NIAMS) grant (AR061430) to K.-H.P.-M. and NIH grants (DE019420, AI044938, and AR050401) to L.B.I. Its contents are solely the responsibility of the authors and do not necessarily represent the official views of the NIH.

References

1. Takayanagi H. Osteoimmunology: shared mechanisms and crosstalk between the immune and bone systems. Nat Rev Immunol. 2007; 7:292–304. [PubMed: 17380158]
2. Lorenzo J, Horowitz M, Choi Y. Osteoimmunology: interactions of the bone and immune system. Endocr Rev. 2008; 29:403–440. [PubMed: 18451259]
3. McInnes IB, Schett G. The pathogenesis of rheumatoid arthritis. N Engl J Med. 2011; 365:2205–2219. [PubMed: 22150039]
4. Novack DV, Teitelbaum SL. The osteoclast: friend or foe? Annu Rev Pathol. 2008; 3:457–484. [PubMed: 18039135]
5. Weilbaecher KN, Guise TA, McCauley LK. Cancer to bone: a fatal attraction. Nat Rev Cancer. 2011; 11:411–425. [PubMed: 21593787]
6. Yasui T, et al. Epigenetic regulation of osteoclast differentiation: possible involvement of Jmjd3 in the histone demethylation of Nfatc1. J Bone Miner Res. 2011; 26:2665–2671. [PubMed: 21735477]
7. Yasui T, Hirose J, Aburatani H, Tanaka S. Epigenetic regulation of osteoclast differentiation. Ann N Y Acad Sci. 2011; 1240:7–13. [PubMed: 22172033]
8. Reik W. Stability and flexibility of epigenetic gene regulation in mammalian development. Nature. 2007; 447:425–432. [PubMed: 17522676]
9. Allis, CD.; Jenuwein, T.; Reinberg, D., editors. Epigentics. Cold Spring Harbor Laboratory Press; New York: 2007.
10. Margueron R, Reinberg D. Chromatin structure and the inheritance of epigenetic information. Nat Rev Genet. 2010; 11:285–296. [PubMed: 20300089]
11. Dawson MA, Kouzarides T. Cancer epigenetics: from mechanism to therapy. Cell. 2012; 150:12–27. [PubMed: 22770212]
12. Arrowsmith CH, Bountra C, Fish PV, Lee K, Schapira M. Epigenetic protein families: a new frontier for drug discovery. Nature reviews Drug discovery. 2012; 11:384–400. [PubMed: 22498752]
13. Belkina AC, Denis GV. BET domain co-regulators in obesity, inflammation and cancer. Nat Rev Cancer. 2012; 12:465–477. [PubMed: 22722403]
14. Nicodeme E, et al. Suppression of inflammation by a synthetic histone mimic. Nature. 2010; 468:1119–1123. [PubMed: 21068722]
15. Dawson MA, et al. Inhibition of BET recruitment to chromatin as an effective treatment for MLL-fusion leukaemia. Nature. 2010; 478:529–533. [PubMed: 21964340]
16. Prinjha RK, Witherington J, Lee K. Place your BETs: the therapeutic potential of bromodomains. Trends Pharmacol Sci. 2012; 33:146–153. [PubMed: 22277300]
17. Filippakopoulos P, et al. Selective inhibition of BET bromodomains. Nature. 2010; 468:1067–1073. [PubMed: 20871596]
18. Zuber J, et al. RNAi screen identifies Brd4 as a therapeutic target in acute myeloid leukaemia. Nature. 2011; 478:524–528. [PubMed: 21814200]
19. Asangani IA, et al. Therapeutic targeting of BET bromodomain proteins in castration-resistant prostate cancer. Nature. 2014
20. Bandukwala HS, et al. Selective inhibition of CD4+ T-cell cytokine production and autoimmunity by BET protein and c-Myc inhibitors. Proc Natl Acad Sci U S A. 109:14532–14537. [PubMed: 22912406]
21. Sasaki H, et al. Effects of combination treatment with alendronate and vitamin K(2) on bone mineral density and strength in ovariectomized mice. J Bone Miner Metab. 2010; 28:403–409. [PubMed: 20101424]
22. Drake MT, Clarke BL, Khosla S. Bisphosphonates: mechanism of action and role in clinical practice. Mayo Clinic proceedings. 2008; 83:1032–1045. [PubMed: 18775204]
23. Ditzel HJ. The K/BxN mouse: a model of human inflammatory arthritis. Trends in molecular medicine. 2004; 10:40–45. [PubMed: 14720585]
24. Ji H, et al. Critical roles for interleukin 1 and tumor necrosis factor alpha in antibody-induced arthritis. J Exp Med. 2002; 196:77–85. [PubMed: 12093872]

25. Wipke BT, Allen PM. Essential role of neutrophils in the initiation and progression of a murine model of rheumatoid arthritis. J Immunol. 2001; 167:1601–1608. [PubMed: 11466382]
26. Charles JF, et al. The collection of NFATc1-dependent transcripts in the osteoclast includes numerous genes non-essential to physiologic bone resorption. Bone. 2012; 51:902–912. [PubMed: 22985540]
27. Negishi-Koga T, Takayanagi H. Ca2+-NFATc1 signaling is an essential axis of osteoclast differentiation. Immunol Rev. 2009; 231:241–256. [PubMed: 19754901]
28. Takayanagi H, et al. Induction and activation of the transcription factor NFATc1 (NFAT2) integrate RANKL signaling in terminal differentiation of osteoclasts. Dev Cell. 2002; 3:889–901. [PubMed: 12479813]
29. Aliprantis AO, et al. NFATc1 in mice represses osteoprotegerin during osteoclastogenesis and dissociates systemic osteopenia from inflammation in cherubism. J Clin Invest. 2008; 118:3775–3789. [PubMed: 18846253]
30. Endo-Munoz L, et al. Loss of osteoclasts contributes to development of osteosarcoma pulmonary metastases. Cancer research. 2010; 70:7063–7072. [PubMed: 20823153]
31. Asagiri M, et al. Autoamplification of NFATc1 expression determines its essential role in bone homeostasis. J Exp Med. 2005; 202:1261–1269. [PubMed: 16275763]
32. Nishikawa K, et al. Blimp1-mediated repression of negative regulators is required for osteoclast differentiation. Proc Natl Acad Sci U S A. 2010; 107:3117–3122. [PubMed: 20133620]
33. Miyauchi Y, et al. The Blimp1-Bcl6 axis is critical to regulate osteoclast differentiation and bone homeostasis. J Exp Med. 2011; 207:751–762. [PubMed: 20368579]
34. Zhao B, Ivashkiv LB. Negative regulation of osteoclastogenesis and bone resorption by cytokines and transcriptional repressors. Arthritis Res Ther. 2011; 13:234. [PubMed: 21861861]
35. Delmore JE, et al. BET bromodomain inhibition as a therapeutic strategy to target c-Myc. Cell. 2011; 146:904–917. [PubMed: 21889194]
36. Battaglino R, et al. c-myc is required for osteoclast differentiation. J Bone Miner Res. 2002; 17:763–773. [PubMed: 12009006]
37. Indo Y, et al. Metabolic regulation of osteoclast differentiation and function. J Bone Miner Res. 2013; 28:2392–2399. [PubMed: 23661628]
38. Huang MJ, Cheng YC, Liu CR, Lin S, Liu HE. A small-molecule c-Myc inhibitor, 10058-F4, induces cell-cycle arrest, apoptosis, and myeloid differentiation of human acute myeloid leukemia. Exp Hematol. 2006; 34:1480–1489. [PubMed: 17046567]
39. Yarilina A, Xu K, Chen J, Ivashkiv LB. TNF activates calcium-nuclear factor of activated T cells (NFAT)c1 signaling pathways in human macrophages. Proc Natl Acad Sci U S A. 2011; 108:1573–1578. [PubMed: 21220349]
40. Schett G. Cells of the synovium in rheumatoid arthritis. Osteoclasts. Arthritis Res Ther. 2007; 9:203. [PubMed: 17316459]
41. Ivashkiv LB, Zhao B, Park-Min KH, Takami M. Feedback inhibition of osteoclastogenesis during inflammation by IL-10, M-CSF receptor shedding, and induction of IRF8. Ann N Y Acad Sci. 2011; 1237:88–94. [PubMed: 22082370]
42. French CA. Pathogenesis of NUT midline carcinoma. Annu Rev Pathol. 2012; 7:247–265. [PubMed: 22017582]
43. Lamoureux F, et al. Selective inhibition of BET bromodomain epigenetic signalling interferes with the bone-associated tumour vicious cycle. Nature communications. 2014; 5:3511.
44. Breuil V, Euller-Ziegler L. Bisphosphonate therapy in rheumatoid arthritis. Joint Bone Spine. 2006; 73:349–354. [PubMed: 16616575]
45. Bouxsein ML, et al. Guidelines for assessment of bone microstructure in rodents using micro-computed tomography. J Bone Miner Res. 2010; 25:1468–1486. [PubMed: 20533309]
46. Park-Min KH, et al. Negative regulation of osteoclast precursor differentiation by CD11b and beta2 integrin-B-cell lymphoma 6 signaling. J Bone Miner Res. 2013; 28:135–149. [PubMed: 22893614]
47. Korganow AS, et al. From systemic T cell self-reactivity to organ-specific autoimmune disease via immunoglobulins. Immunity. 1999; 10:451–461. [PubMed: 10229188]

48. Kitaura H, et al. M-CSF mediates TNF-induced inflammatory osteolysis. J Clin Invest. 2005; 115:3418–3427. [PubMed: 16294221]

49. Parfitt AM, et al. Bone histomorphometry: standardization of nomenclature, symbols, and units. Report of the ASBMR Histomorphometry Nomenclature Committee. J Bone Miner Res. 1987; 2:595–610. [PubMed: 3455637]

50. Melville KM, et al. Female mice lacking estrogen receptor-alpha in osteoblasts have compromised bone mass and strength. J Bone Miner Res. 2014; 29:370–379. [PubMed: 24038209]

51. Seal J, et al. Identification of a novel series of BET family bromodomain inhibitors: binding mode and profile of I-BET151 (GSK1210151A). Bioorg Med Chem Lett. 2012; 22:2968–2972. [PubMed: 22437115]

52. Mirguet O, et al. From ApoA1 upregulation to BET family bromodomain inhibition: discovery of I-BET151. Bioorg Med Chem Lett. 2012; 22:2963–2967. [PubMed: 22386529]

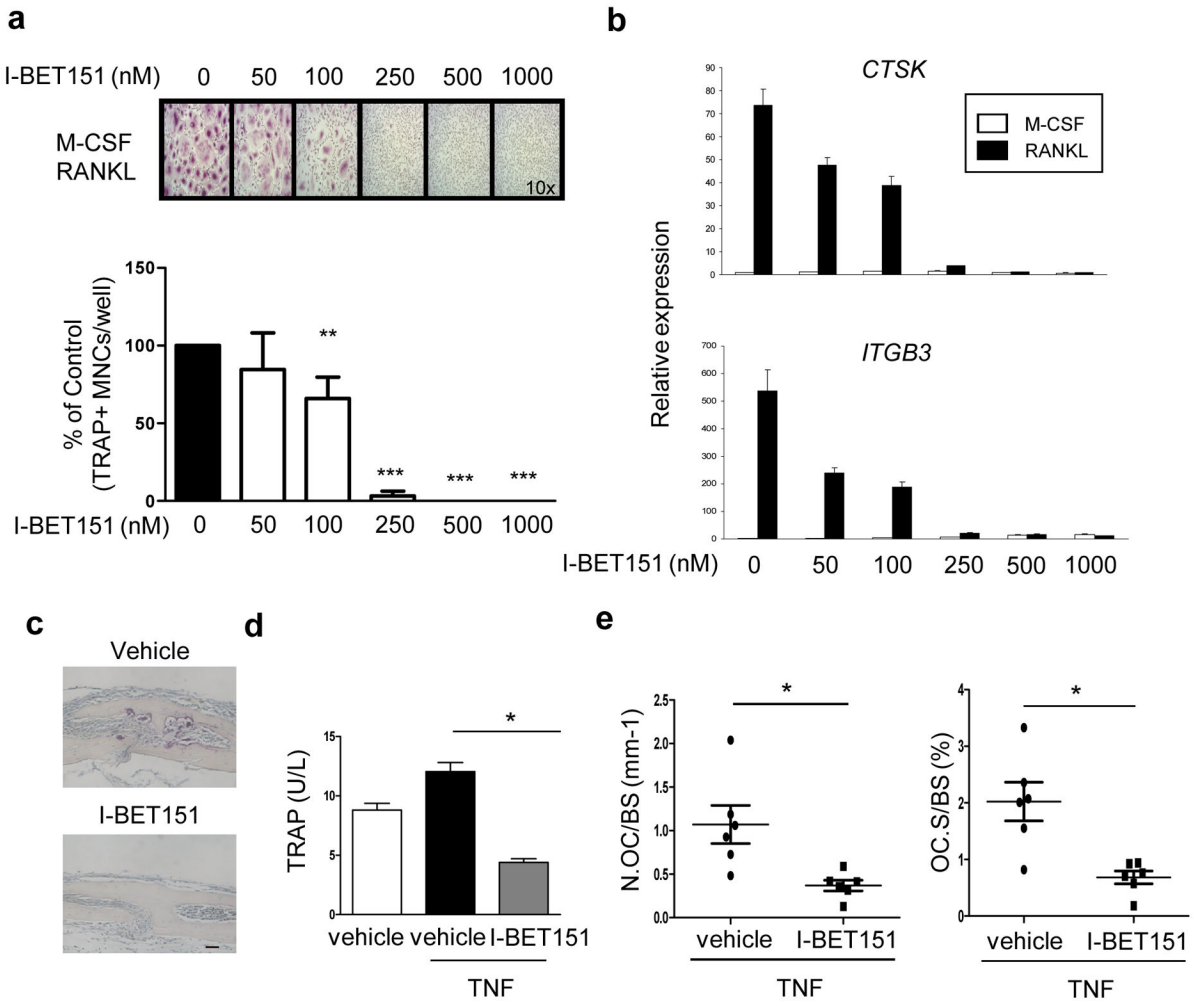

Figure 1. I-BET151 inhibits osteoclastogenesis

a. Human OCPs ($CD14^+$ monocytes cultured overnight with M-CSF (20 ng ml^{-1})) were treated with DMSO (vehicle control, labeled 0) or I-BET151 at the indicated concentrations for 1hr prior to addition of RANKL (40 ng ml^{-1}). After 5 days of culture, TRAP-positive, multinucleated (more than three nuclei) cells were counted in triplicate. The number of osteoclasts generated by RANKL alone is set as 100% for each individual blood donor. *Upper panel*, Representative results from one of more than three experiments. *Lower panel*, Data are shown as mean ± SEM from aggregate data from 9 independent donors. **: $P < 0.01$, ***: $P < 0.001$ by two-way ANOVA. **b.** Human OCPs were cultured as in **a** for 5 days and mRNA was measured using real-time PCR. mRNA levels were normalized relative to GAPDH mRNA. Representative results from at least three independent experiments are shown. **c–e.** TNF-induced osteolysis model. TNF (70 μg per kg body weight) was injected over calvarial periosterium for four consecutive days, during which time either vehicle control or I-BET151 (40 mg kg^{-1} body weight) in 10 % KLEPTOSE® was administrated intraperitoneally (i.p.) once per day. Data shown are from 6 mice per group. **c.** TRAP staining of histological sections obtained from control or I-BET151 treated mice after supracalvarial TNF administration. Scale bar: 100 μm. **d.** ELISA measurement of serum

TRAP. *: $P < 0.05$ by one-way ANOVA. **e**. Histomorphometric analysis. Osteoclast number per bone surface (N.Oc BS^{-1}). Osteoclast surface area per bone surface (OcS BS^{-1}). All data are shown as mean ± SEM. *:$P < 0.05$ by *t*-test.

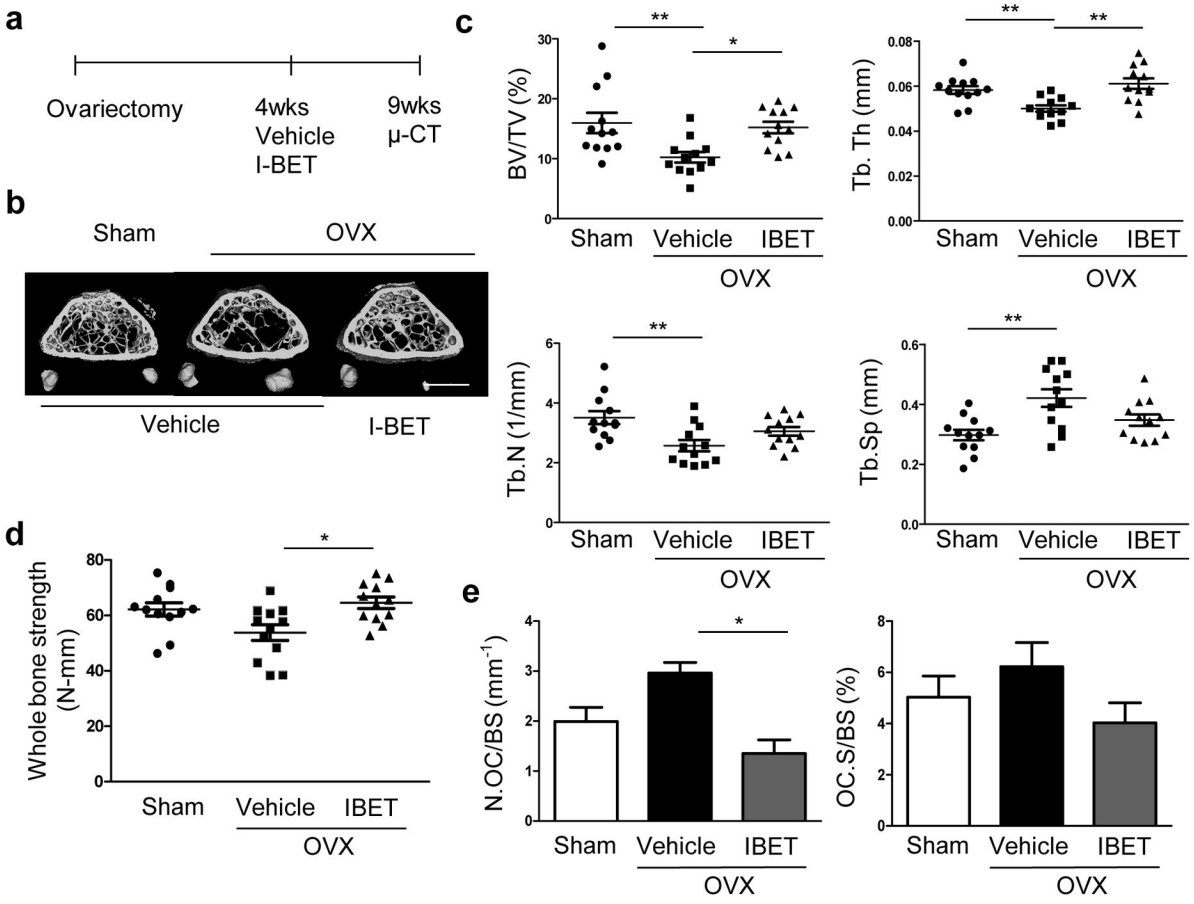

Figure 2. I-BET 151 increases bone mass and strength in ovariectomized mice

a. A schematic diagram illustrating the therapeutic experimental design. **b–c.** Therapeutic effect of the BET bromodomain protein inhibitor, I-BET151 on post ovariectomy bone loss (n=12 per group). Sham-operated mice (Sham). **b.** Representative images showing trabecular architecture by micro-computed tomography (μCT) reconstruction in the distal femurs. Scale bars, 1 mm. **c.** μCT measurements for the indicated parameters in distal femurs. Bone volume (BV/TV), trabecular space (Tb.Sp.), trabecular number (Tb.N.) and trabecular thickness (Tb.Th.) were determined by μCT analysis. **d**. 3-point bending test of femurs. **e.** Histomorphometric analysis of tibia. Osteoclast number per bone surface (N.Oc BS^{-1}). Osteoclast surface area per bone surface (OcS BS^{-1}). All data are shown as mean ± SEM * P <0.05, ** P <0.01. One-way ANOVA with a posthoc Tukey test was performed.

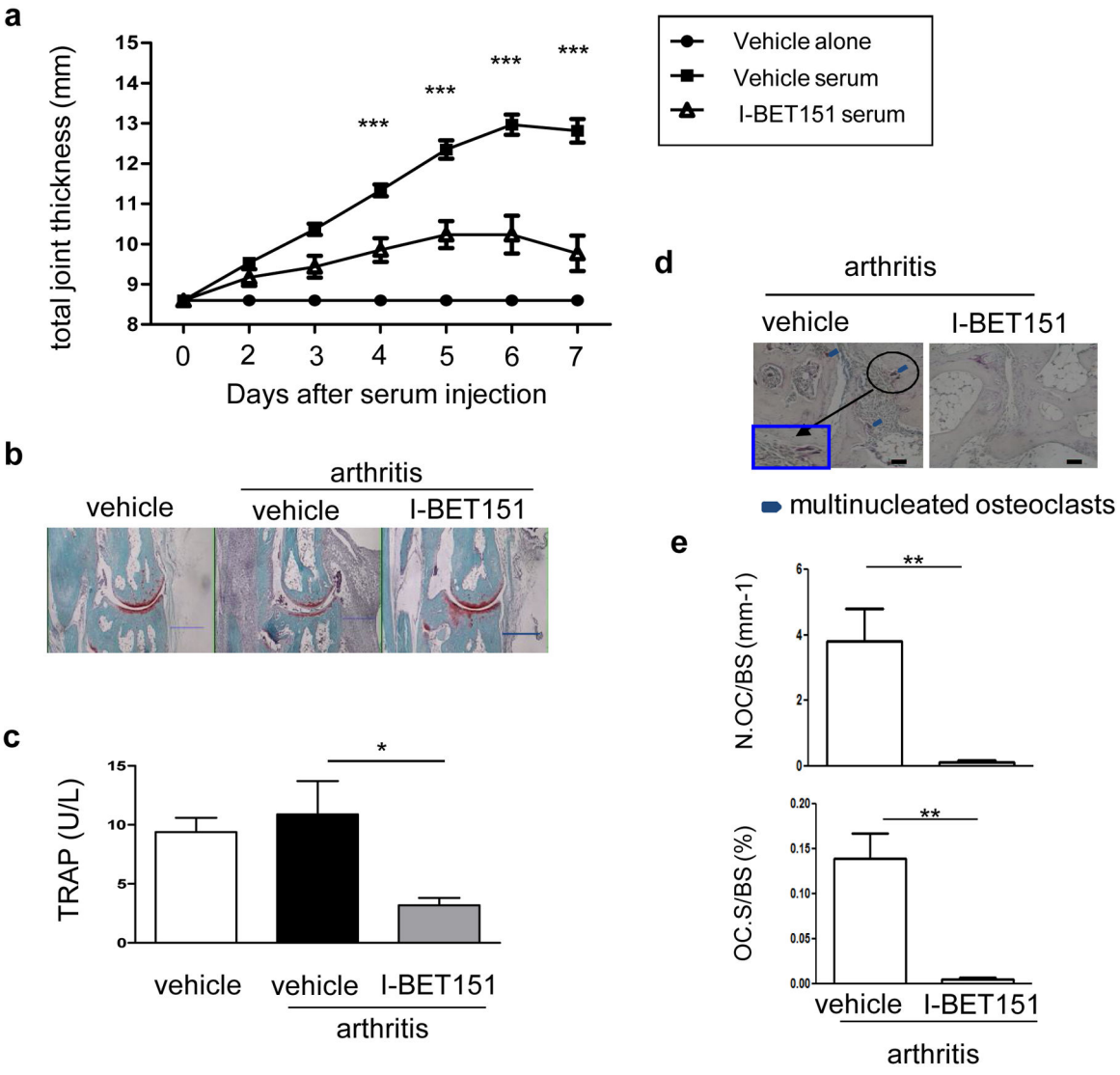

Figure 3. I-BET151 attenuates K/BxN serum–induced arthritis

Arthritis was induced in C57BL/6 mice and I-BET151 was administered as described in Methods. **a.** Time course of joint swelling in the presence and absence of I-BET151 treatment. Values are the mean ± SEM of 6 mice per group. ***: $P < 0.001$ by two-way ANOVA. **b.** Histology of ankle joints of mice examined 11 days after the first arthritogenic serum injection. Hind paws were fixed and decalcified, and ankle joint sections were prepared and stained with hematoxylin, fast green, and Safranin O. Scale bar: 500μm **c.** Serum TRAP levels were measured 7 days after arthritis induction. *: $P < 0.05$ by two-way ANOVA. **d.** TRAP staining of histological sections obtained from control or I-BET151 treated arthritic mice. Blue square (inset) shows an enlarged image. Scale bar:100μm **e.** Histomorphometric analysis. Osteoclast number per bone surface (N.Oc BS^{-1}). Osteoclast surface area per bone surface (OcS BS^{-1}). All data are shown as mean ± SEM. *:$P < 0.05$ by *t*-test.

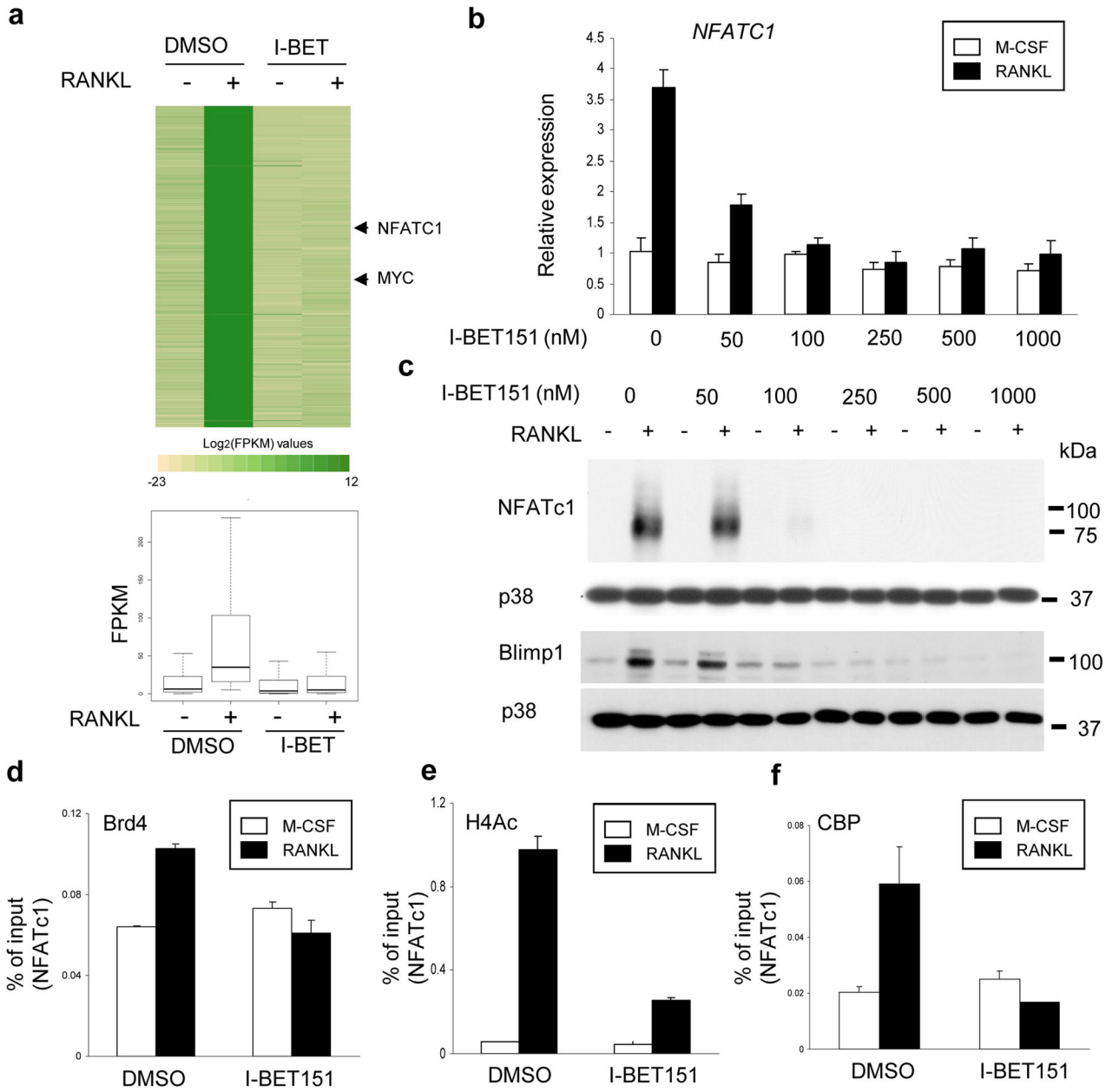

Figure 4. I-BET151 inhibits *NFATC1* expression

Human OCPs were treated with DMSO or I-BET151 for 1 hr, and then cultured with RANKL (40 ng ml^{-1}) for one day. **a.** upper panel: Heat map of RNA-seq FPKM values for 465 genes which were induced > 2-fold by RANKL and whose expression was suppressed by >50% by I-BET151 in two independent donors as shown Supplementary Fig. 8. Lower panel: box plot depicting FPKM values. (n=2) **b.** mRNA was measured using real-time PCR and normalized relative to GAPDH mRNA. Results are shown as means ± SD of triplicate determinants. **c.** Immunoblot of whole-cell lysates using NFATc1, Blimp1 and p38 antibodies. Same samples were loaded into two gels and p38 was served as a loading control for each gel. Suppression of NFATc1 expression by I-BET151 was observed in at least 10

independent experiments. Images have been cropped for presentation; full size blots are shown in Supplementary Figure 18. **d–f.** Human OCPs were treated with DMSO (vehicle control) or I-BET151 (500 nM) for 1 hr, and RANKL (40ng ml^{-1}) was added for additional 24 hrs. Chromatin immunoprecipitation (ChIP) analysis of the NFATC1 promoter for Brd4 (**d**), acetylated H4 (**e**), or CBP (**f**). All data are shown as mean ± SD. Representative results from at least three independent experiments are shown.

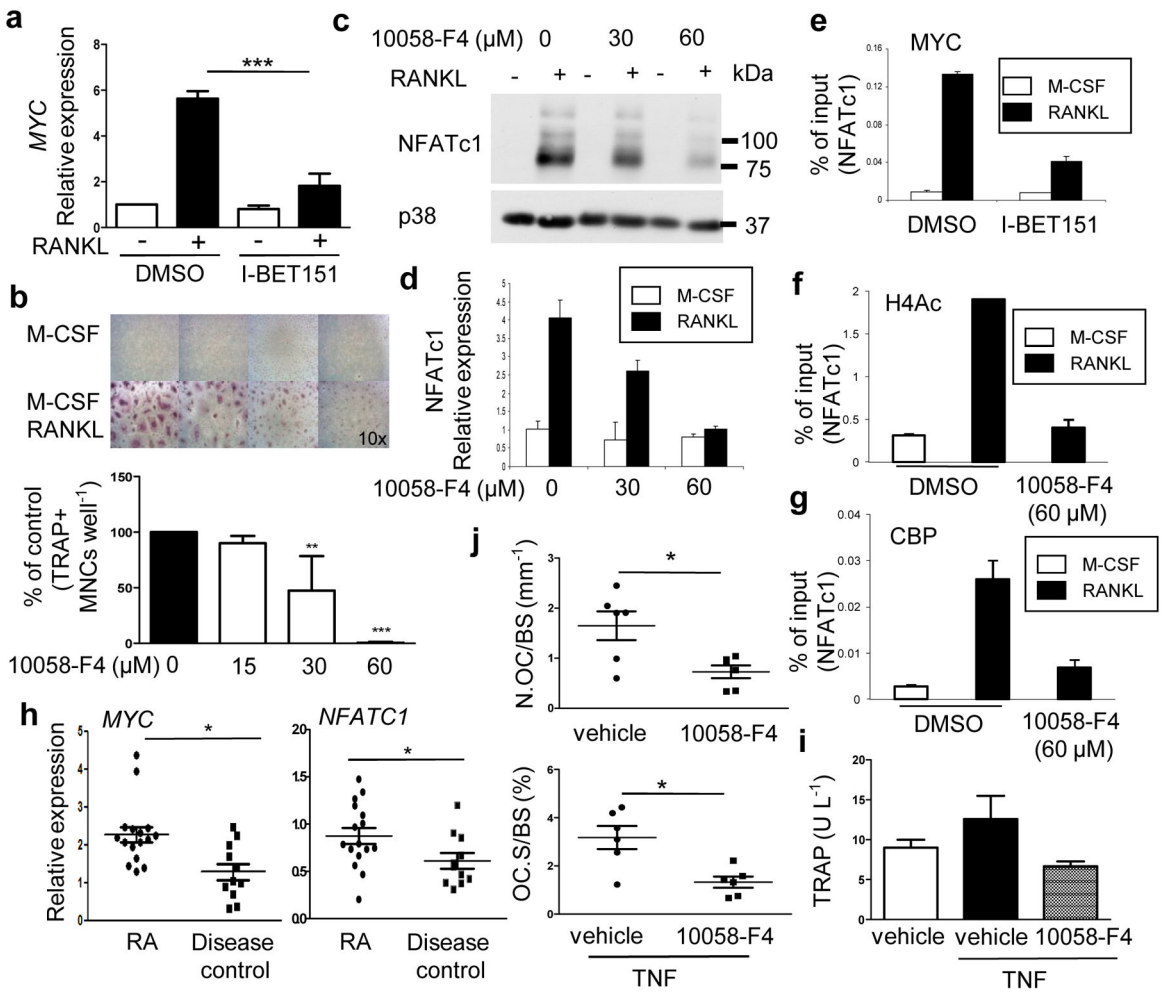

Figure 5. I-BET151 suppresses RANKL-induced MYC expression

a. Human OCPs were treated with DMSO or I-BET151 at the indicated concentrations for 1 hr, and then cultured with RANKL (40 ng ml^{-1}) for one day (n=4). Analysis of expression of MYC mRNA by real time-PCR. All data are shown as mean ± SEM. ***:$P < 0.001$ by One-way ANOVA. **b.** (n=4) Osteoclastogenesis assay. Human OCPs were cultured with either DMSO (vehicle control) or 10058-F4 at the indicated doses for 1 hr prior to RANKL stimulation, and TRAP-positive multinucleated (more than three nuclei) cells were counted 5 days after RANKL addition. *Upper panel*, Representative results obtained from one donor are shown. *Lower panel*, Data are shown as means ± SEM. **c–d.** Cells were cultured with 10058-F4 at the indicated doses for 1hr, and RANKL was then added for 2 days. **c.** Immunoblot of whole cell lysates with NFATc1 and p38 antibodies. Images have been cropped for presentation; full size blots are shown in Supplementary Figure 18. **d.** *NFATc1* mRNA was measured by real-time PCR. mRNA levels were normalized to the expression of GAPDH. **e–g.** ChIP analysis for MYC (**e**), acetylated H4 (**f**), or CBP (**g**) at the *NFATC1* promoter in human OCPs. Representative results from three independent experiments are shown. All data are shown as mean ± SD. **h.** MYC and NFATC1 expression in RA synovial macrophages mRNA from synovial CD14^{+} cells from rheumatoid arthritis patients (n=16)

or sero-negative arthritis disease control patients (n=11) was measured using real-time PCR. mRNA levels were normalized relative to the expression of GAPDH. All data are shown as mean ± SEM.*: $P < 0.05$; by *t*-test. **i–j.** TNF-induced supracalvareal osteolysis. n=6. TNF (83 μg per kg body weight) was injected over calvarial periosterium for five consecutive days, and either vehicle (DMSO) or 10058-F4 (30 mg kg^{-1}) was administrated intraperitoneally (i.p.) once per day. **i.** The concentration of serum TRAP measured by ELISA. **j.** Histomorphometric analysis of calvaria from either vehicle or 10058-F4 treated mice; osteoclast number per bone surface (N.Oc BS^{-1}) and osteoclast surface area per bone surface (OcS BS^{-1}). All data are shown as mean ± SEM. *:$P < 0.05$ by *t*-test.